Carbohydrate Polymers 90 (2012) 875–886

Contents lists available at SciVerse ScienceDirect

Carbohydrate Polymers

journal homepage: www.elsevier.com/locate/carbpol

Fixed-bed column studies on a modified chitosan hydrogel for detoxification of aqueous solutions from copper (II)

Iman Kavianinia[a,*], Paul G. Plieger[a], Nadia G. Kandile[b], David R.K. Harding[a]

[a] Chemistry, Institute of Fundamental Sciences, Massey University, Palmerston North, New Zealand
[b] Department of Chemistry, Faculty for Women, Ain Shams University, Heliopolis, Cairo, Egypt

ARTICLE INFO

Article history:
Received 8 May 2012
Received in revised form 8 June 2012
Accepted 9 June 2012
Available online 17 June 2012

Keywords:
Biosorption
Crosslinked chitosan
Packed-bed column
Copper ions

ABSTRACT

A new efficient, low cost chitosan based biosorbent was successfully prepared and employed for the biosorption of copper ions from an aqueous solution using a fixed bed column. Pyromellitic dianhydride crosslinked chitosan as the new adsorbent was characterized by SEM, FTIR spectroscopy, X-ray diffraction, thermogravimetric analysis and solid state ^{13}C NMR analysis. Scanning electron microscopy coupled with an X-ray energy dispersed analysis for the copper-equilibrated biomass confirmed the presence of Cu(II) ions on the surface of the hydrogel. Thermogravimetric analysis showed a significant improvement in the thermal stability of the new hydrogel compared to pure chitosan. Kinetic models were applied to predict the breakthrough curves. This study shows that the prepared hydrogel based on modified chitosan could be utilized as an efficient bioadsorbent for the removal of copper ions from wastewater.

1. Introduction

Biosorption, using either living or dead biomass, has emerged in the last decade as one of the most promising techniques for metal removal (Mcafee, Gould, Nadeau, & da Costa, 2001; Muzzarelli, 2011). Chitosan is the partly acetylated (1-4)-2-amino-2-deoxy-β-D-glucan obtained from chitin (Muzzarelli, 1977). Due to its promising characteristics that include biocompatibility, hydrophilicity, biodegradability and anti-bacterial properties, chitosan has received wide spread attention (Chung & Chen, 2008; Muzzarelli et al., 2012; Rajiv Gandhi, Kousalya, Viswanathan, & Meenakshi, 2011). Despite these numerous properties and characteristics, chitosan (Cts) has not been used on an industrial scale for waste water treatment due to its unsatisfactory mechanical properties, poor heat resistance, dissolution in acidic media and high swelling ratios. In addition, hydrodynamic limitations and column fouling become important issues. One way to improve the physicochemical properties of a chitosan matrix is to introduce various functional groups on the surface of chitosan such as glutaraldehyde and epichlorohydrin (Bratskaya et al., 2012; Jin, Song, & Hourston, 2004).

In order to begin addressing these issues, we have previously synthesized, a chitosan based adsorbent with high mechanical and chemical stability. We crosslinked chitosan with aromatic dianhydrides (Kavianinia, Plieger, Kandile, & Harding, 2012). Aromatic polyimides which in general are comprised of five-membered heterocyclic imide bonds have received much attention for their excellent characteristics including thermal stability, chemical resistance, excellent electrical properties, high glass transition temperature, high modulus and mechanical integrity (So, Cho, & Sahoo, 2007). These properties are influenced by the nature of the moiety originating from the aromatic dianhydride (Majumdar & Biswas, 1990). Therefore, we propose the introduction of five-membered heterocyclic imide rings to the chitosan backbone to develop the physicochemical properties of the matrix.

Copper ions can be found in the aqueous waste streams of many industries such as electronics, plating, mining, paper and pulp, wire drawing, wood production and phosphate fertilizer production (Li & Bai, 2005). Excessive intake of copper by man leads to severe mucosal irritation, central nervous system irritation, liver and kidney failure and death (Liu, Deng, Zhan, & Zhang, 2002). As a result, elevated copper concentrations in the environment over recent decades have received increasing concern by the public. Up to now, numerous techniques have been available for the removal of copper from aqueous solutions including chemical precipitation, ion exchange, membrane filtration, electrolytic methods, and reverse osmosis (Qiu & Zheng, 2009). These methods however, have several disadvantages such as high operational cost, ineffective removal of trace levels of heavy metal ions and generation of polluted byproducts (Reddad, Gerente, Andres, & Le Cloirec, 2002; Wan Ngah, Endud, & Mayanar, 2002; Zhou, Wang, Liu, & Huang, 2009)

* Corresponding author at: Chemistry, Turitea Campus, Palmerston North, Private Bag 11222, Palmerston North 4442, New Zealand. Tel.: +64 6 3569099; fax: +64 6 3542140.
E-mail address: i.kavianinia@massey.ac.nz (I. Kavianinia).

0144-8617/$ – see front matter © 2012 Elsevier Ltd. All rights reserved.
http://dx.doi.org/10.1016/j.carbpol.2012.06.014

It has been shown that chitosan cross-linked with glutaraldehyde, perhaps the most popular hydrogel crosslinker, exhibits a reduced matrix thermal stability as compared to pure chitosan (Neto et al., 2005). We propose here that the use of the inexpensive pyromellitic dianhydride (PMDA) for hydrogel crosslinking will aid in the thermal stability of the chitosan matrix as we aim for industrial applications.

The objective of the present investigation is to examine the performance of chitosan–PMDA for the removal of Cu(II) ions from aqueous solutions in a fixed-bed system as well as to evaluate its physical properties. There are numerous batch studies performed on the removal of heavy metals using chitosan or its derivatives, with only a few studies reported on a packed bed column system (Futalan, Kan, Dalida, Pascua, & Wan, 2011). The effect of influent concentration, bed height and flow rate on column performance and the shape of the breakthrough curves were evaluated. Adams–Bohart, Thomas and Yoon–Nelson models were applied to the experimental data to evaluate the dynamic performance of the adsorption process and to assist in predicting the breakthrough curves. Regeneration of the chitosan–PMDA was also conducted using 0.1 mol L^{-1} HCl to assess whether the biomass was able to be efficiently regenerated and reused.

2. Materials and methods

2.1. Reagents

Analytical grade copper (II) sulfate ($CuSO_4{\cdot}5H_2O$) was obtained from May and Baker, Australia. Hydrochloric acid and sodium hydroxide used for pH adjustment, chitosan, with an average molecular weight of 600,000 and an 83% degree of deacetylation and pyromellitic dianhydride (PMDA) were obtained from the Aldrich Chemical Company.

2.2. Chemical modifications of the biomass

Chitosan (2.00 g, 0.0124 mol of glucosamine residues) was dispersed in glacial acetic acid (40 mL) and shaken well for 1 h then added to PMDA (8.00 g, 0.036 mol) dissolved in DMF (100 mL). The reaction mixture was heated at 130 °C for 24 h. The precipitate was filtered off, washed with DMF, methanol and deionized water and then dried in a vacuum.

2.3. Instrumentation

The FTIR spectra of the chitosan derivatives as KBr discs were recorded with a Nicolet 5700 FTIR spectrometer. Elemental analysis was performed using a Carlo Erba Elemental Analyser EA 1108 using a flash combustion technique. The X-ray diffraction patterns were recorded on a Rigaku RAxisIV++ image-plate detector using a multi-metal-layer Osmic confocal optic to monochromate and focus the Cu Kα radiation produced by a Rigaku MM007 micro-focus rotating-anode generator. Data were collected and analysed using the Crystal Clear program (v.1.4.0). Solid-state carbon-13 (^{13}C) magic angle spinning (MAS) NMR spectra were obtained at a ^{13}C frequency of 50.3 MHz on a Bruker (Rheinstetten, Germany) DRX 200 MHz spectrometer. The surface morphology of the powders was studied using an FEI Quanta 200 Scanning Electron Microscope (Eindhoven, The Netherlands) at an accelerating voltage of 20 kV. A TA Instruments SDT Q600 instrument was used for simultaneous DTG and TGA data acquisition. Data were analyzed using TA Universal Analysis software.

2.4. Column studies

The experiments were carried out using a glass column with an internal diameter of 1 cm and a height of 30 cm. Glass wool was placed on both ends of the column to prevent washing out and/or floating up of the adsorbent. Glass beads were also provided on top of the column to allow for even distribution of the influent. The pH of the inlet solution was set to 6.0. Effluent samples were collected at predetermined time intervals. The metal concentration in the effluent solution was determined by a GBC model 903 flame atomic absorption spectrophotometer. All measurements were carried out in an air/acetylene flame. The wavelength and current of Cu(II) was 324.7 and 5 mA, respectively. A peristaltic pump P-1 (Pharmacia Fine Chemicals) was used to provide a constant flow rate for metal adsorption and desorption solution in the fixed bed column.

2.4.1. Effect of bed depth

The sorption performance of modified chitosan was studied at bed heights of 1 cm and 2 cm. The flow rate of 0.20 mL min^{-1} and the initial influent concentration of 50 mg L^{-1} of copper were kept constant.

2.4.2. Effect of influent Cu(II) concentration

The effect of inlet copper concentration (50 mg L^{-1}, 100 mg L^{-1} and 200 mg L^{-1}) on the adsorption performance of modified chitosan was analysed. A bed height of 1 cm and a flow rate of 0.20 mL min^{-1} were kept constant.

2.4.3. Effect of flow rate

The effect of flow rates of 0.20 mL min^{-1} and 0.40 mL min^{-1} on copper sorption by modified chitosan was studied. The initial inlet concentration and bed height was held constant at 50 mg L^{-1} and 1 cm, respectively.

2.5. Analysis of column data

The column bed performance is usually determined from the breakthrough curve. The time for appearance and the shape of the breakthrough curve are very important characteristics for determining the operation and dynamic response of a sorption column (Hatzikioseyian, Tsezos, & Mavituna, 2001). Experimental determination of these parameters is very dependent on column operating conditions such as flow rate, inlet concentration and bed height. The breakthrough curve shows the loading behaviour of metal to be removed from solution in a fixed-bed and is usually expressed as the ratio of effluent metal concentration to inlet metal concentration C_t/C_0 as a function of time or volume of the effluent for a given bed height (Aksu & Gonen, 2004).

The breakthrough time t_b (min) and the saturation or exhaustion time t_e (min) were used to evaluate the mass transfer zone (Δt) given by:

$$\Delta t = t_e - t_b \tag{1}$$

The length of the mass transfer zone (Z_m), can be computed from the breakthrough curve as follows:

$$Z_m = Z\left(\frac{1 - t_b}{t_e}\right) \tag{2}$$

where Z is the bed height (cm).

The effluent volume, V_{eff} (mL), can be calculated from the following equation:

$$V_{\text{eff}} = Qt_{\text{total}} \tag{3}$$

where Q and t_{total} are the volumetric flow rate (mL min^{-1}) and the total flow time (min), respectively.

The total amount of Cu(II) applied to column can be calculated from Eq (4):

$$m_{\text{total}} = \frac{C_0 Q t_{\text{total}}}{1000} \quad (4)$$

Total metal removal percent of Cu(II) with respect to flow volume can be calculated as follows:

$$\%\,\text{removal} = \frac{q_{\text{total}}}{m_{\text{total}}} \times 100 \quad (5)$$

The quantity of metal retained in the column, q_{total} (mg) can be calculated from the area under the plot of the adsorbed Cu(II) concentration C_{ad} ($C_{\text{ad}} = C_0 - C$) (mg L^{-1}) versus effluent time (t, min) and is calculated through numerical integration:

$$q_{\text{total}} = \frac{QA}{1000} = \frac{Q}{1000} \int_{t=0}^{t=t_{\text{total}}} C_{\text{ad}}\, dt \quad (6)$$

where t_{total}, Q and A are the total flow time (min), volumetric flow rate (mL min^{-1}) and the area under the breakthrough curve, respectively.

Equilibrium metal uptake (q_{eq}) (or maximum capacity of the column) in the column is defined by Eq. (7) as the total amount of metal sorbed (q_{total}) per gram of sorbent (X) at the end of total flow time.

$$q_{\text{eq}} = \frac{q_{\text{total}}}{X} \quad (7)$$

3. Results and discussion

3.1. Preparation of the hydrogel

The imidization reaction mechanism involves the nucleophilic attack of the amino group of the chitosan on the carbonyl carbon of the anhydride group. This equilibrium reaction involves opening of the anhydride ring to form an amic acid intermediate. However, the following reaction to form the imide has a rate constant of several orders of magnitude larger than the reverse reaction (Lavrov, Ardashnikov, Kardash, & Pravednikov, 1977). Dipolar aprotic solvents, in this study DMF, prevent dissociation of the carboxyl proton, which can reverse the reaction through hydrogen bonding with the carboxyl group. The amide acid formation is exothermic (Ghosh & Mittal, 1996). Therefore the cyclization of the ortho-carboxyamide intermediate through nucleophilic attack of the amide nitrogen on the acid carbonyl carbon with elimination of water can be readily attained by thermal imidization.

The degree of substitution (DS) was calculated as 87% on the basis of the percentage of nitrogen in the product by the following equation (Jančiauskaitė & Makuška, 2008):

$$\text{DS} = \left(\frac{N - 8.26}{1162/(143 + M) + 238/(185 + M - 8.38)} \right) \times 100 \quad (8)$$

where N is the percentage of nitrogen content and M is the molecular weight of dianhydride.

3.2. Characterization

3.2.1. Fourier transform infrared spectroscopy

In this study, FTIR analysis was employed to investigate the characteristic chemical structure of the chitosan and the crosslinked chitosan (chitosan–PMDA). The FTIR results for the crosslinked chitosans and unmodified chitosan are shown in Fig. 1. The major peaks for the chitosan in Fig. 1a can be attributed as follows: 3447.5 cm^{-1} the overlapping of O—H stretching and N—H stretching bands, 2879.9 cm^{-1} the CH stretching vibration in —CH and —CH_2, 1659 and 1598.2 cm^{-1} the amide C=O bond of the remaining acetamido groups and N—H bending vibration of —NH_2 groups, respectively, 1424.8 cm^{-1} can be assigned to the —NH deformation vibration in —NH_2, 1384.6 cm^{-1} CH the symmetric bending vibration in —CHOH, 1325 and 1155.5 cm^{-1} C—N the stretching vibration and 1081.5 and 1033 cm^{-1} the —CO stretching vibration in —COH. After modification of chitosan, the spectra (Fig. 1b) showed some major changes. The characteristic bands of symmetrical C=O stretching and unsymmetrical C=O stretching of the imide group were clearly visible at 1721.2 cm^{-1} and 1778.9 cm^{-1}, respectively.

3.2.2. Elemental analysis

The elemental analyses were found C, 41.66%; H, 7.77%; N, 7.83% and C, 47.19%; H, 4.60%; N, 4.25% for chitosan and modified chitosan, respectively. It was noted that modification of chitosan decreased the percentage of nitrogen. This is due to the dianhydride crosslinking agent reacting with the —NH_2 groups and increasing the amount of carbon, oxygen and hydrogen in the hydrogel relative to nitrogen. The percentage of free amine groups on the chitosan was determined by elemental analysis using the following equation (Kasaai, Arul, & Charlet, 2000):

$$\text{DD} = \left(\frac{1 - (\text{C/N}) - 5.145}{6.861 - 5.145} \right) \times 100 \quad (9)$$

where 5.145 is related to completely N-deacetylated chitosan ($C_6H_{11}O_4N$ repeat unit) and 6.861 is the fully N-acetylated polymer ($C_8H_{13}O_5N$ repeat unit). The degree of deacetylation of the chitosan used in this study was 83%.

3.2.3. X-ray diffraction analysis

2D-XRD patterns of chitosan and its derivatives are shown in Fig. 2. The diffractogram of chitosan, Fig. 2a, shows two main crystalline peaks at 2θ values of 9.60° and 19.28° that are generally assigned to weak chain–chain ordering of the chitosan chains, in addition to several weak crystalline peaks in agreement with the characteristic diffractogram of the unmodified chitosan (Nunthanid, Puttipipatkhachorn, Yamamoto, & Peck, 2001). This diffraction pattern shows the partially crystalline structure of chitosan. These diffraction signals at $2\theta = 9.6°$ ($d \sim 9.2$ Å) and 19.3° ($d \sim 4.6$ Å) were not observed in the XRD patterns of Fig. 2b, which indicates that the chemical crosslinking between chitosan and PMDA destroys the crystallinity of chitosan and increases the amorphous volume in the modified chitosan hydrogel. The reduction in the crystallinity of chitosan after modification is evidence for irregular packing of chitosan subunits as a result of the crosslinking (Monteiro & Airoldi, 1999). The substitution of amino groups by PMDA causes a reduction of the strong hydrogen bonding that is found in the unmodified chitosan. Chitosan–PMDA, Fig. 2b, shows a single very broad weak band at ~19° indicating vestiges of the parent chitosan structure. The weak low-angle diffraction feature at ~9.5° is generally assigned to weak lengthwise ordering between chitosan subunits. The weak feature at ~12° is assigned to an increase in separation between chains caused by this rigid linker.

3.2.4. Solid state ^{13}C NMR analysis

The analysis of the ^{13}C DP-MAS spectrum of chitosan (Fig. 3a) shows signals at 55.9(C2), 59.3(C6), 83.4(C4) of the pyranose ring. A well defined signal is observed at 74.9 ppm, which could be assigned to overlapping C3 and C5. The signal due to the C1 carbon, which is directly attached to two oxygen atoms, was found at 104.8 ppm which is at a significantly lower magnetic field value compared with the signals of the remaining five carbons (Saito, Tabeta, & Ogawa, 1987). After grafting the PMDA to the chitosan backbone, new resonance is observed, (Fig. 3b). The signals at 115–140 ppm are attributed to the phenylene ring. A well defined signal is observed at 165.8 ppm, which can be assigned to the carbonyl group carbon of the imide ring.

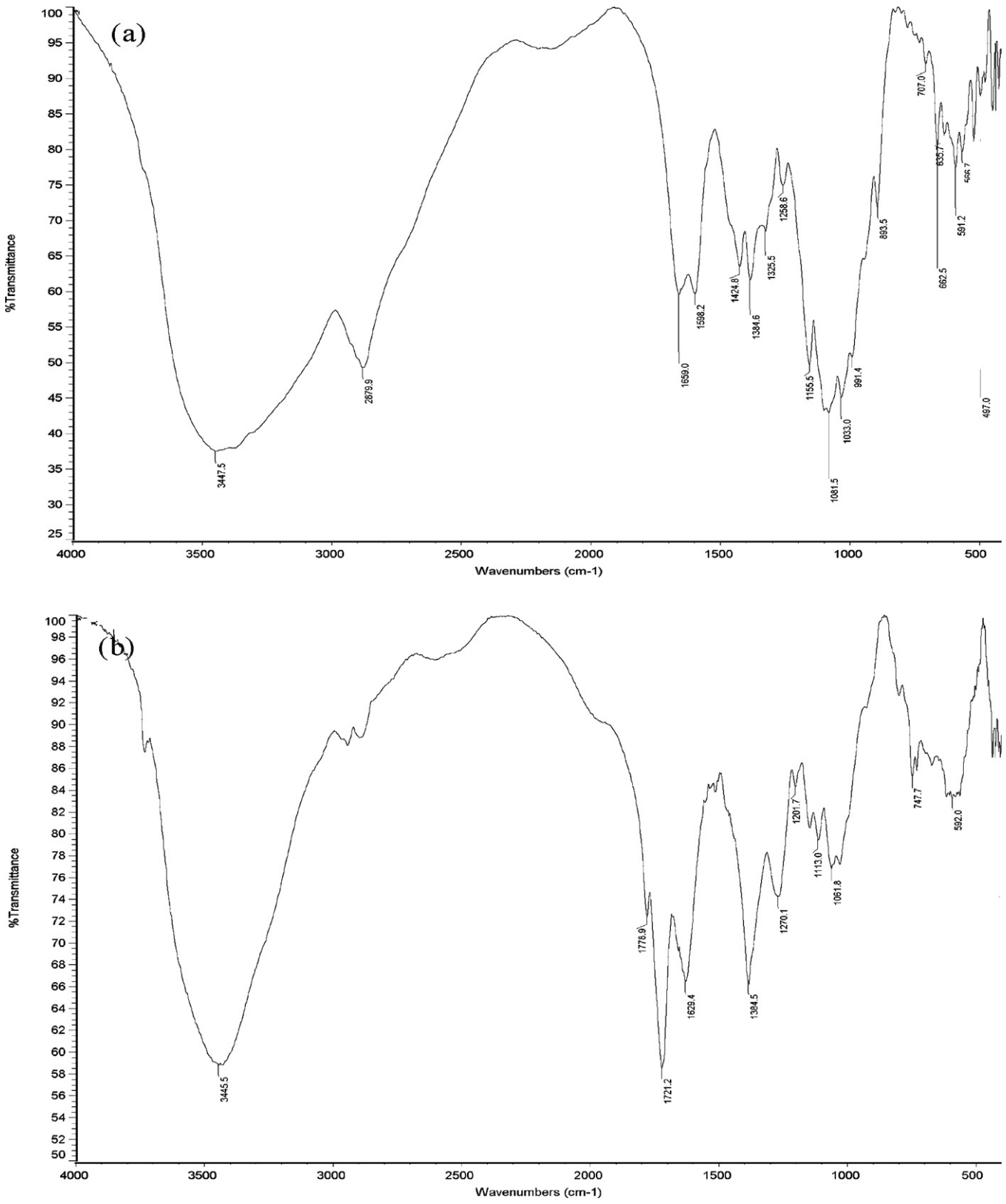

Fig. 1. FTIR spectra of (a) Cts and (b) Cts–PMDA.

3.2.5. Scanning electron microscopy (SEM)

Fig. 4 illustrates scanning electron micrographs of the surface of (a) chitosan and (b) chitosan–PMDA, respectively. Fig. 4a and b represents pure chitosan powder, which displays a smooth surface. Fig. 4c and d shows that significant morphological changes have occurred after modification of chitosan with PMDA. The agglomerated and irregular surface structure of the modified chitosan shows that the chitosan has been chemically modified.

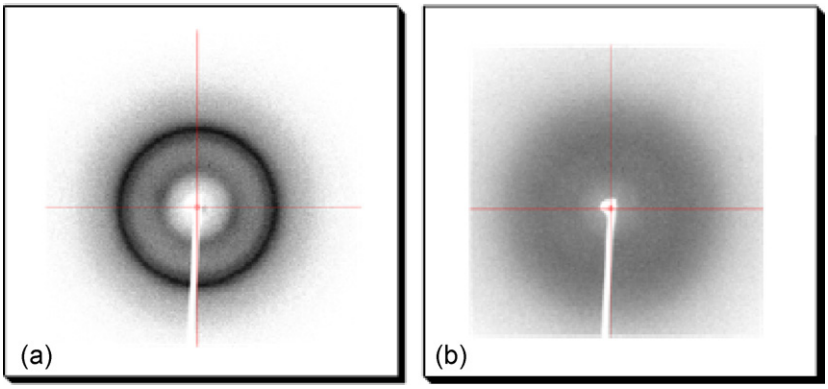

Fig. 2. 2D-XRD of (a) Cts and (b) Cts–PMDA.

3.2.6. Energy dispersive analysis of X-rays (EDAX)

Scanning electron microscopy coupled with X-ray energy dispersed analysis before and after metal removal was undertaken in order to confirm the presence of Cu(II) ions in the hydrogel. EDAX spectra of the unloaded hydrogels and the copper-loaded hydrogels are shown in Fig. 5. In the case of virgin chitosan powder (Fig. 5a), the characteristic peak of copper ion was not present. In the case of copper ion-adsorbed chitosan–PMDA matrix (Fig. 5b), the peak of copper ion is clearly shown.

3.2.7. Thermal gravimetric analysis and differential thermal gravimetric analysis (TGA/DTG)

The degradation and thermal stability behavior of chitosan and chitosan–PMDA were evaluated by TGA under a nitrogen atmosphere (Fig. 6). The TGA of chitosan revealed. weight loss occurs in two distinct stages. Firstly, weight loss of 11% in a temperature range between 42 and 142 °C occurs for Cts due to loss of adsorbed and bound water. The weight loss of 5% for chitosan–PMDA hydrogels indicated a slightly lower adsorbance of moisture as might be expected from the aromatic crosslinker. The second weight loss of Cts begins at about 220 °C relating to degradation of the chitosan. Thermal decomposition is more marked in the region between 235 and 356 °C with a weight loss of 38%. For the crosslinked polymer a lower weight loss (22%) as compared to unmodified chitosan (44%) at the same temperature (300 °C) provides proof that crosslinking of Cts with PMDA had decreased the rate of degradation and a degree of increased thermal stability had been achieved. More accurate differences of the thermal behavior of the chitosan and Cts–PMDA can be noted from the DTG curves. The DTG peak of chitosan showed a maximum value of about 282 °C, while the maximum value of this peak for the Cts–PMDA curve is observed at about 313 °C showing the increase in the thermal stability of the Cts–PMDA over chitosan.

As might be predicted from the characteristics of aromatic anhydrides used in synthetic polymers (Bessonov, 1987), the crosslinking of chitosan with pyromellitic dianhydride increased the thermal stability of chitosan.

3.3. Influence of operating conditions on column sorption of copper ions

3.3.1. Effect of column bed depth

To study the effect of bed depth on the adsorption performance of the matrix experiments were conducted with two columns filled with different bed heights (1 cm and 2 cm) with a constant influent concentration of 50 mg L^{-1} and flow rate of 0.20 mL min^{-1} (Fig. 7a). A longer breakthrough time (t_b) and exhaustion time (t_e) was observed when the bed depth was increased to 2 cm. The effluent volume (V_{eff}) also increased with an increase in bed depth, which would be due to the greater contact time. Table 1 shows that total Cu(II) ion removal (%) increased with increasing bed height which would due to increased adsorbent surface area, which provided more binding sites for the column adsorption. Thus modification of chitosan with PMDA does not alter the matrix significantly with respect to the expected chromatographic behaviour yet it improves its thermal stability.

3.3.2. Effect of influent Cu(II) concentration

The effect of inlet ion concentration on the breakthrough curves at bed height 1 cm and flow rate 0.2 mL min^{-1} is given in Fig. 7b. In Table 1, when the initial Cu(II) ion concentration increased from 50 to 100 mg L^{-1}, Cu(II) adsorption removal decreased from 52% to 32%. At the higher metal concentration (100 mg L^{-1}) the bed saturated more quickly leading to earlier breakthrough and exhaustion time. Table 1 shows that highest uptake is obtained at the higher metal concentration which would be due to high influent Cu(II) ion concentration providing higher driving force for the transfer process to overcome the mass transfer resistance.

The volume of the influent was also decreased from 435 mL to 375 mL as the influent concentration was increased from 50 mg L^{-1} to 100 mg L^{-1}.

3.3.3. Effect of flow rate

The influence of flow rate on the biosorption of Cu(II) by modified chitosan was investigated by keeping the influent metal concentration (50 mg L^{-1}) and the bed height (1 cm) constant and varying the flow rate. The plot of dimensionless concentration (C_t/C_0) versus time (t) at different flow rates is shown in Fig. 7c. As would be expected an increased rate produced a faster breakthrough. The breakthrough time, exhaustion time and uptake capacity decreased as the flow rate increased due to decrease in the residence time of the solute in the column.

3.3.4. Comparison of adsorption capacity with other adsorbents

In order to justify the viability of the treatment process, the adsorptive capacities of these sorbents must be compared with other sorbents examined for the treatment of Cu(II) ions under similar conditions. Comparison of chitosan–PMDA with other adsorbent materials is difficult owing to different experimental conditions used in each case. The adsorption capacities of adsorbents collected from the literature are listed in Table 2. Our results are included for comparison. It can be seen that chitosan–PMDA exhibits promising results. High adsorption capacity and high chemical stability of Cts–PMDA positions this novel hydrogel as a strong candidate for utilizing chitosan based adsorbents in industrial applications.

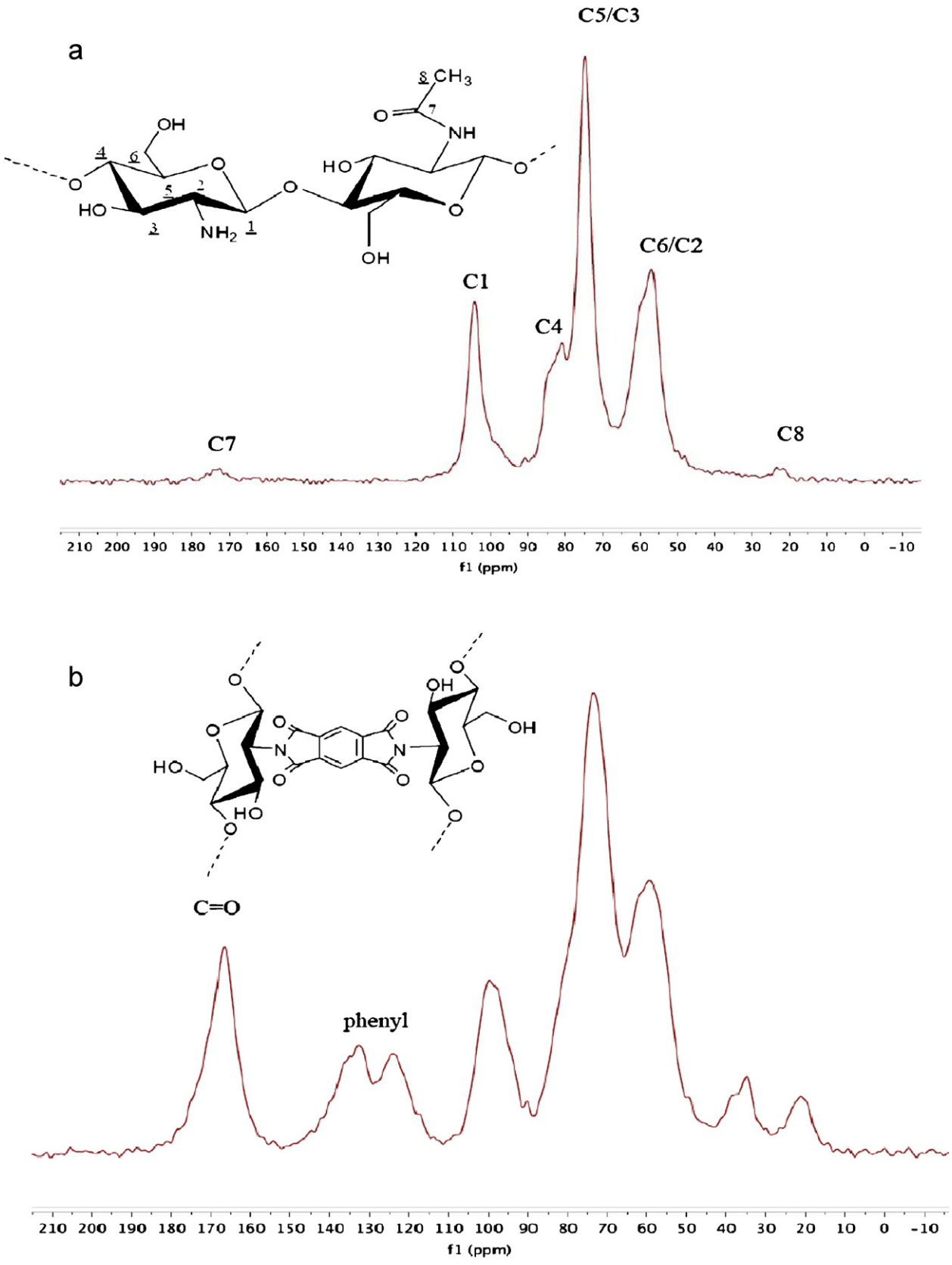

Fig. 3. ^{13}C DP-MAS spectra of (a) Cts and (b) Cts–PMDA.

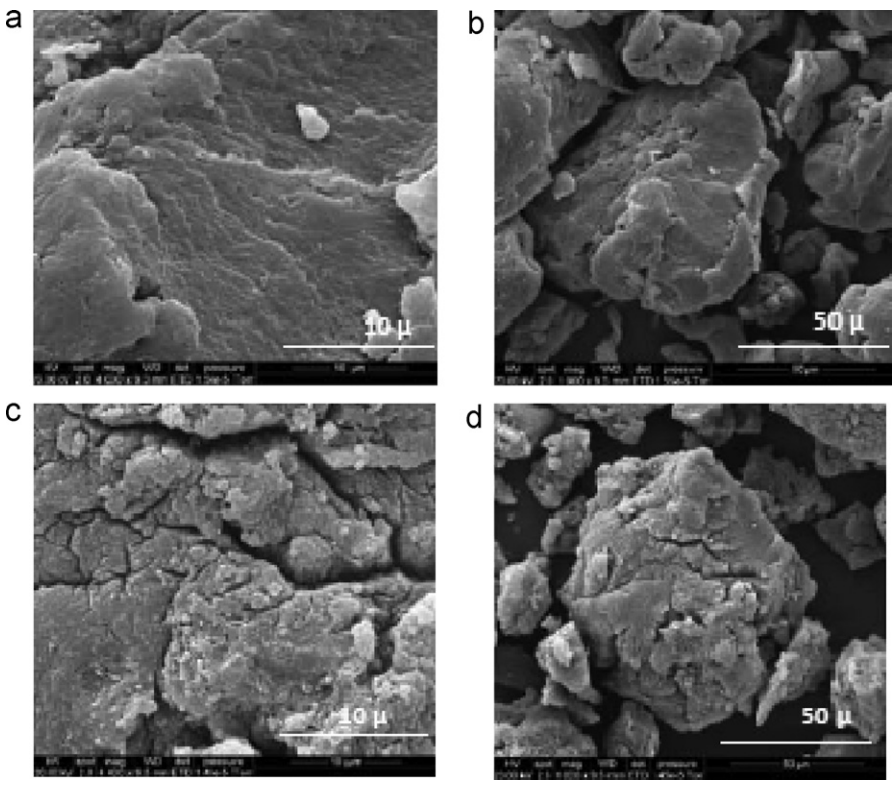

Fig. 4. SEM of (a and b) Cts and (c and d) Cts–PMDA.

Table 1
Column data and parameters in fixed-bed column for Cu(II) ion adsorption by modified Cts.

Operational parameters	Adsorption parameters						
	Δt (min)	q_{total} (mg)	q_{eq} (mg g^{-1})	m_{total} (mg)	V_{eff} (mL)	Total Cu removal (%)	Z_m (cm)
Different influent concentration[a]							
50 mg L^{-1}	1575	11	39	21	435	52	0.72
100 mg L^{-1}	1525	12	40	37	375	32	0.81
Different bed height[b]							
1 cm	1575	11	39	21	435	52	0.72
2 cm	3325	27	45	50	1000	54	0.66
Different flow rate[c]							
0.20 mL min^{-1}	1575	11	39	21	435	52	0.72
0.40 mL min^{-1}	1025	8	29	21	420	42	0.80

[a] Z = 1 cm; Q = 0.20 mL min^{-1}.
[b] C_0 = 50 mg L^{-1}; Q = 0.20 mL min^{-1}.
[c] Z = 1 cm; C_0 = 50 mg L^{-1}.

3.4. Breakthrough curve modelling

Several mathematical models have been developed for describing and analyzing lab-scale column studies for the purpose of industrial applications. In this study, the Adams–Bohart, Thomas and Yoon models were used to identify the best model for predicting the dynamic behaviour of the column.

3.4.1. Adams–Bohart model

Although the original model of Adams–Bohart was applied to a gas–charcoal adsorption system, its overall approach can be applied successfully in the quantitative description of other systems. The Adams–Bohart model assumes that the adsorption rate is proportional to both the residual capacity of the sorbent and the concentration of the sorbing species. This is used only for the

Table 2
Comparative adsorption capacity of different adsorbents for Cu(II) ion removal.

Adsorbent	Q (mg g^{-1})	Inlet concentration (mg L^{-1})	Flow (mL min^{-1})	Bed height (cm)	References
Cts–PMDA	39	50	0.2	1	Present work
Iron oxide-coated zeolite	12.4	60	11	6	Han et al. (2009)
Green coconut shell	41	100	2	10	Sousa et al. (2010)
Rice husk based activated carbon	29.34	15	10	1	Yahaya et al. (2011)
Chitosan glutaraldehyde nanoparticles	0.042	0.5	0.3	3	Futalan et al. (2011)
Chitosan immobilized on bentonite	21.3	500	0.2	1.3	Futalan et al. (2011)

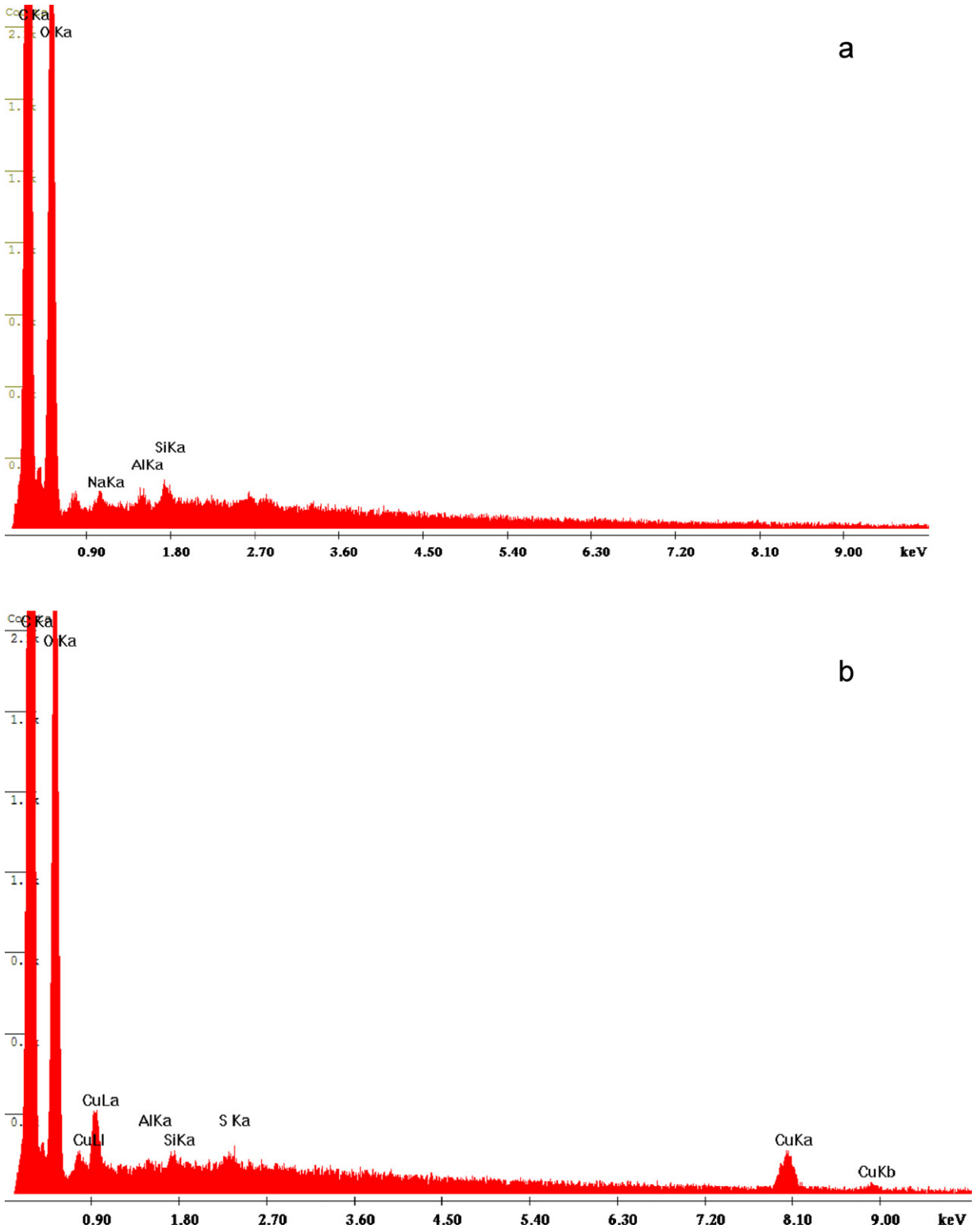

Fig. 5. EDAX plots of unloaded (a) and loaded Cts–PMDA (b).

description of the initial part of the breakthrough curve (Han et al., 2008). The expression used is as follows:

$$\frac{\ln C_t}{C_0} = k_{AB}C_0 t - k_{AB}N_0\frac{Z}{U_0} \quad (10)$$

where C_t is the effluent concentration of adsorbate in the liquid phase (mg L^{-1}); C_0 is initial concentration of sorbate in the liquid phase (mg L^{-1}), N_0 is the sorption capacity (mg L^{-1}), k_{AB} is the kinetic constant (L mg^{-1} min^{-1}), U_0 is the superficial velocity (cm min^{-1}) defined as the ratio of the volumetric flow rate Q (cm^3 min^{-1}) to the cross-sectional area of the bed A (cm^2) and Z is the bed depth of the fixed bed column (cm). The model constants k_{AB} and N_0 were calculated and are presented in Table 3 from a plot of between $\ln C_t/C_0$ against t at given flow rate, bed

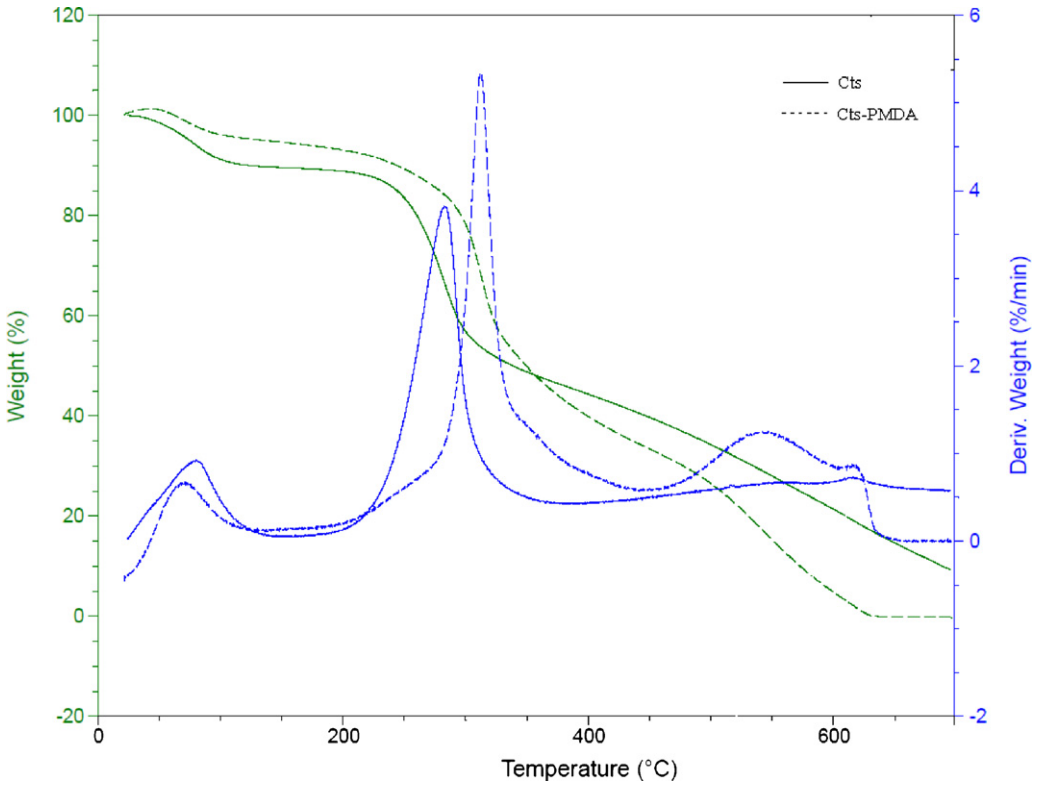

Fig. 6. TGA/DTG of Cts and Cts–PMDA.

height and inlet copper concentrations. The values of k_{AB} increased with both initial metal concentration and flow rate increase but it decreased with bed depth increase. This shows that the overall system kinetics were dominated by external mass transfer in the initial part of adsorption in the column. The predicted curves from the Adams–Bohart model were compared with the corresponding experimental data at different experimental conditions (Fig. 7). There is good agreement between the experimental data and predicted values.

3.4.2. Thomas model

The Thomas model is one of the most widely used models to describe the performance theory of the sorption process in a fixed-bed column. This model assumes that Langmuir kinetics of adsorption–desorption and no axial dispersion arre derived with the assumption that the rate driving force obeys second-order reversible reaction kinetics (Thomas, 1944). The linearized form of the Thomas model is as follows (Futalan et al., 2011):

$$\ln\left(\frac{C_0}{C}-1\right)=\frac{k_{th}q_0X}{Q}-\frac{k_{TH}C_0}{Q}V_{eff} \quad (11)$$

where Q is the flow rate (mg L^{-1}), X is the mass of adsorbent (g), V_{eff} is the volume of effluent treated (mL), q_0 is the maximum solid phase concentration of solute (mg g^{-1}) and k_{TH} is the Thomas rate constant (mL [mg min]$^{-1}$). The 'k_{TH}' and 'q_0' value were calculated by plotting $\ln(C_t/C_0-1)$ against 't' using values from the column experiments and the results are presented in Table 3. From the regression coefficient R^2, it can be concluded that the Thomas model provided a better fit compared to the Adams–Bohart model. It can be seen that as flow rate increased, the value of k_{TH} increased whereas the value of 'q_0' showed a reverse trend. With bed depth increasing, the value of k_{TH} decreased and the value of q_0 increased. The bed capacity q_0 increased and the coefficient k_{TH} decreased with the increase in initial Cu(II) ion concentration. This was attributed to the driving force for adsorption in the concentration difference. Thus the lower flow rate, higher influent concentration and higher bed depth would increase the adsorption of Cu(II) ion. The Thomas model was suitable for the adsorption process, which indicated that the external and internal diffusions were not the limiting steps.

3.4.3. Yoon and Nelson model

Yoon and Nelson (1984) developed a model to investigate the adsorption and breakthrough of adsorbate vapours or gases with respect to activated charcoal. The Yoon and Nelson model is based on the assumption that the rate of decrease in the probability of adsorption for each adsorbate molecule is proportional to the prob-

Table 3
Adams–Bohart, Thomas and Yoon–Nelson model parameters at different conditions using linear regression analysis.

C_0 (mg L^{-1})	Q (mL min^{-1})	Z (cm)	Adams–Bohart			Thomas			Yoon–Nelson		
			k_{AB}, 10^{-4} (L mg^{-1} min^{-1})	N_0 (mg L^{-1})	R^2	k_{TH}, 10^{-4} (mL mg^{-1} min^{-1})	q_0 (mg g^{-1})	R^2	k_{YN}, 10^{-2} (min^{-1})	τ (min)	R^2
50	0.2	1	0.2	25,703	0.907	0.84	38	0.964	0.42	1151	0.964
50	0.2	2	0.18	23,111	0.919	0.36	46	0.959	0.19	2701	0.989
50	0.4	1	0.54	11,800	0.895	1.3	28	0.993	0.66	428	0.993
100	0.2	1	0.35	23,727	0.889	0.65	48	0.991	0.65	642	0.991

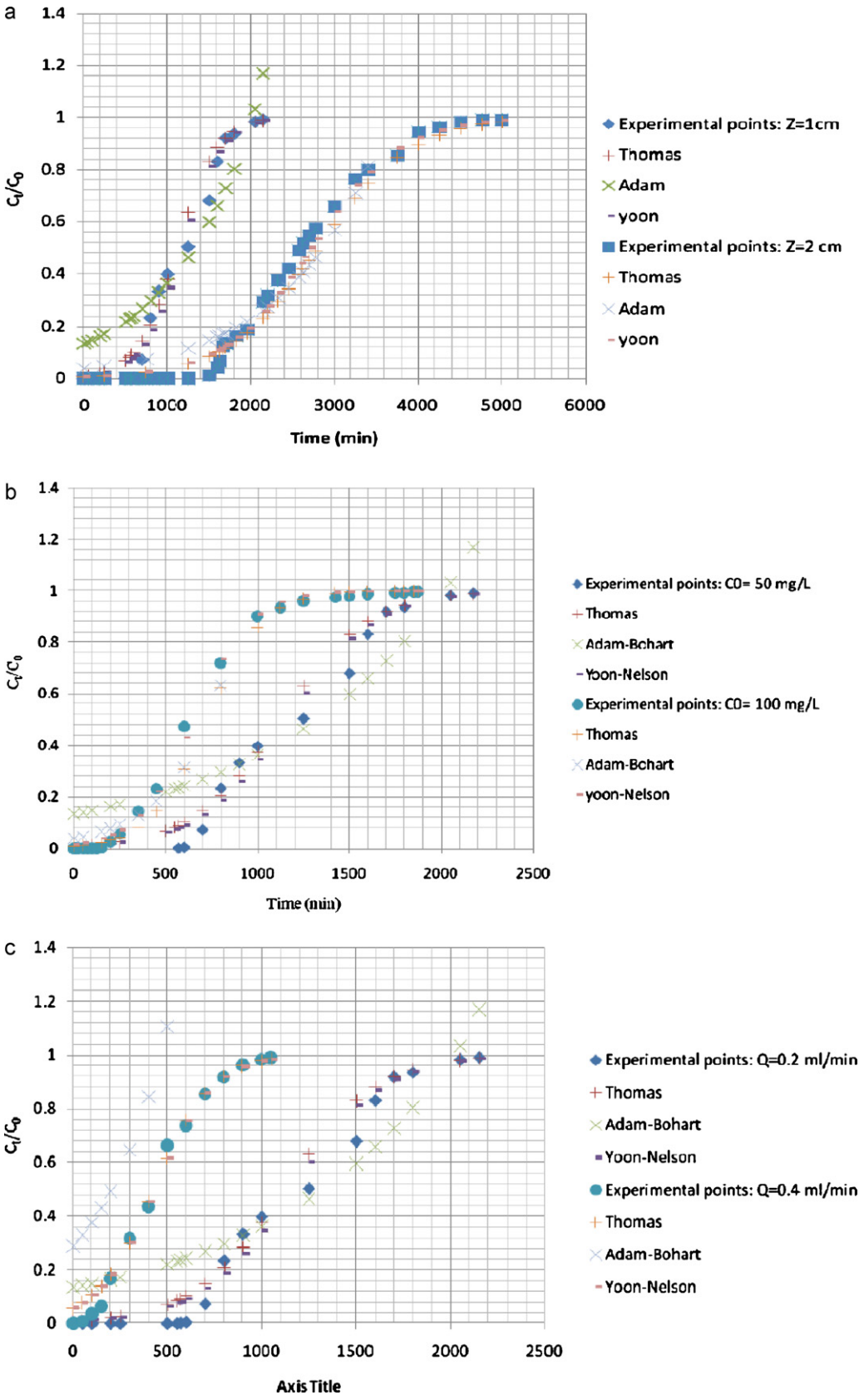

Fig. 7. Experimental and predicated breakthrough curves of Cu(II) adsorption into Cts–PMDA at (a) different bed depths (C_0 = 50 mg L^{-1}, Q = 0.2 mL min^{-1}), (b) different initial concentration (Z = 1 cm, Q = 0.2 mL min^{-1}) and (c) different flow rates (C_0 = 50 mg L^{-1}, Z = 1 cm).

Table 4
Sorption process parameter for two sorption–desorption cycles.

Cycle	q_e (mg g^{-1})	t_b (min)	t_e (min)	Δt	Total removal (%)
1	38.67	400	2800	2600	41.44
2	36.16	250	2625	2375	41.33

ability of adsorbate adsorption and the probability of adsorbate breakthrough on the adsorbent (Kundu & Gupta, 2007). The Yoon and Nelson equation for a single component system is expressed as:

$$\ln\left(\frac{C_t}{C_0 - C}\right) = k_{YN}t - \tau k_{YN} \quad (12)$$

where k_{YN} is the rate constant (min^{-1}) and τ is the time required for 50% adsorbate breakthrough (min).

The values of 'k_{YN}' and 'τ' were estimated from the plot between $\ln(C_t/C_0 - C_t)$ versus 't' at different flow rates, bed heights and initial Cu(II) ion concentrations (Table 3).

As seen in the table, the values of k_{YN} were found to increase with increase in both flow rate and Cu(II) ion influent concentration. On the other hand, with the bed volume increasing the values of τ increased while the values of k_{YN} decreased. Among those models, the Thomas and Yoon and Nelson model was found to be most suitable to represent the kinetics of biosorption of Cu(II) ion in a fixed bed of chitosan–PMDA.

3.4.4. Column regeneration

Reusability of the sorbent is of crucial importance in any industrial practice for metal removal from wastewater. This can be evaluated by comparing the sorption performance of regenerated biomass with the original biomass. In this study, modified chitosan was reused for two sorption–desorption cycles at 0.2 mL min^{-1}. The column was packed with 0.3 g of modified chitosan yielding an initial bed height of 1 cm and saturated with 50 mg L^{-1} initial Cu(II) concentration. The adsorption mechanism of Cu(II) on any adsorbent can be physical, chemical bonding, ion-exchange or a combination of all three. If adsorption is by physical bonding, then the loosely bound Cu(II) ions can be easily desorbed in aqueous solution. However, if the adsorption process is through chemical bonding, ion-exchange or a combination of both, then desorption can be affected by the use of stronger eluents like acidic or alkaline solutions. Therefore, attempts were made to desorb Cu(II) from the loaded adsorbent using 0.1 M HCl solution at the same flow rate. The concentration of Cu(II) was monitored with time. This process was repeated twice. As shown in Table 4, a decreased breakthrough time was observed from 400 min to 250 min.

4. Conclusion

A new efficient, cheap chitosan based bioadsorbent with increased thermal stability was synthesized and used for removal of Cu(II) from an aqueous solution in a fixed bed column. The results obtained showed that the sorption Cu(II) is dependent on the bed height, flow rate, and influent concentration. A longer breakthrough and exhaustion time occurred at a higher bed height, a lower flow rate and lower influent concentration. The Adams–Bohart, the Thomas, and the Yoon–Nelson models were successfully applied to the experimental data obtained from dynamic studies performed on a fixed column to predict the breakthrough curves and to determine the column kinetic parameters.

Acknowledgements

We would like to acknowledge Dr Jason Hindmarsh, Institute of Food, Nutrition & Human Health, Massey University, Palmerston North, New Zealand for his assistance and providing access to the solid-state NMR spectrometer.

References

Aksu, Z., & Gonen, F. (2004). Biosorption of phenol by immobilized activated sludge in a continuous packed bed: Prediction of breakthrough curves. *Process Biochemistry*, *39*, 599–613.
Bessonov, M. I. (1987). *Polyimides thermally stable polymers*. New York and London: Consultants Bureau., p. 76.
Bratskaya, S. Y., Azarova, Y. A., Matochkina, E., Kodess, M., Yatluk, Y. G., & Pestov, A. (2012). N-(2-(2-pyridyl) ethyl) chitosan: Synthesis, characterization and sorption properties. *Carbohydrate Polymers*, 869–875.
Chung, Y. C., & Chen, C. Y. (2008). Antibacterial characteristics and activity of acid-soluble chitosan. *Bioresource Technology*, *99*, 2806–2814.
Futalan, C. M., Kan, C. C., Dalida, M. L., Pascua, C., & Wan, M. W. (2011). Fixed-bed column studies on the removal of copper using chitosan immobilized on bentonite. *Carbohydrate Polymers*, *83*, 697–704.
Ghosh, M. K., & Mittal, K. L. (1996). *Polyimides: Fundamentals and applications*. New York: CRC, Marcel Dekker.
Han, R., Ding, D., Xu, Y., Zou, W., Wang, Y., Li, Y., et al. (2008). Use of rice husk for the adsorption of congo red from aqueous solution in column mode. *Bioresource Technology*, *99*, 2938–2946.
Han, R., Zou, L., Zhao, X., Xu, Y., Xu, F., Li, Y., et al. (2009). Characterization and properties of iron oxide-coated zeolite as adsorbent for removal of copper (II) from solution in fixed bed column. *Chemical Engineering Journal*, *149*(1–3), 123–131.
Hatzikioseyian, A., Tsezos, M., & Mavituna, F. (2001). Application of simplified rapid equilibrium models in simulating experimental breakthrough curves from fixed bed biosorption reactors. *Hydrometallurgy*, *59*, 395–406.
Jančiauskaitė, U., & Makuška, R. (2008). Polyelectrolytes from natural building blocks: Synthesis and properties of chitosan-o-dextran graft copolymers. *Chemija*, *19*, 35–42.
Jin, J., Song, M., & Hourston, D. (2004). Novel chitosan-based films cross-linked by genipin with improved physical properties. *Biomacromolecules*, *5*, 162–168.
Kasaai, M. R., Arul, J., & Charlet, G. (2000). Intrinsic viscosity–molecular weight relationship for chitosan. *Journal of Polymer Science Part B: Polymer Physics*, *38*, 2591–2598.
Kavianinia, I., Plieger, P. G., Kandile, N. G., & Harding, D. R. K. (2012). New hydrogels based on symmetrical aromatic anhydrides: Synthesis, characterization and metal ion adsorption evaluation. *Carbohydrate Polymers*, *87*, 881–893.
Kundu, S., & Gupta, A. (2007). As (III) removal from aqueous medium in fixed bed using iron oxide-coated cement (IOCC): experimental and modeling studies. *Chemical Engineering Journal*, *129*(1–3), 123–131.
Lavrov, S., Ardashnikov, A. Y., Kardash, I. Y., & Pravednikov, A. (1977). Cyclization of aromatic poly(amic acids) to polyimides. Cyclization kinetics of a model compound of N-phenylphthalamic acid. *Polymer Science USSR*, *19*, 1212–1219.
Li, N., & Bai, R. (2005). Copper adsorption on chitosan–cellulose hydrogel beads: Behaviors and mechanisms. *Separation and Purification Technology*, *42*, 237–247.
Liu, M., Deng, Y., Zhan, H., & Zhang, X. (2002). Adsorption and desorption of copper (II) from solutions on new spherical cellulose adsorbent. *Journal of Applied Polymer Science*, *84*, 478–485.
Majumdar, A., & Biswas, M. (1990). Thermal stability, dielectric and conductivity characteristics of 9,10-anthracene-diol-anhydride polycondensates. *Polymer Bulletin*, *24*, 565–572.
Mcafee, B. J., Gould, W. D., Nadeau, J. C., & da Costa, A. C. A. (2001). Biosorption of metal ions using chitosan, chitin, and biomass of *Rhizopus oryzae*. *Separation Science and Technology*, *36*, 3207–3222.
Monteiro, O. A. C., Jr., & Airoldi, C. (1999). Some studies of crosslinking chitosan–glutaraldehyde interaction in a homogeneous system. *International Journal of Biological Macromolecules*, *26*, 119–128.
Muzzarelli, R. A. A. (1977). *Chitin*. Oxford: Pergamon Press., pp. 220–228.
Muzzarelli, R. A. A. (2011). Potential of chitin/chitosan-bearing materials for uranium recovery: An interdisciplinary review. *Carbohydrate Polymers*, *84*, 54–63.
Muzzarelli, R. A. A., Boudrant, J., Meyer, D., Manno, N., DeMarchis, M., & Paoletti, M. G. (2012). Current views on fungal chitin/chitosan, human chitinases, food preservation, glucans, pectins and inulin: A tribute to Henri Braconnot, precursor of the carbohydrate polymers science, on the chitin bicentennial. *Carbohydrate Polymers*, *87*, 995–1012.
Neto, C. G. T., Giacometti, J., Job, A., Ferreira, F., Fonseca, J., & Pereira, M. (2005). Thermal analysis of chitosan based networks. *Carbohydrate polymers*, *62*(2), 97–103.
Nunthanid, J., Puttipipatkhachorn, S., Yamamoto, K., & Peck, G. E. (2001). Physical properties and molecular behavior of chitosan films. *Drug Development and Industrial Pharmacy*, *27*, 143–157.

Qiu, W., & Zheng, Y. (2009). Removal of lead, copper, nickel, cobalt, and zinc from water by a cancrinite-type zeolite synthesized from fly ash. *Chemical Engineering Journal*, *145*, 483–488.

Rajiv Gandhi, M., Kousalya, G., Viswanathan, N., & Meenakshi, S. (2011). Sorption behaviour of copper on chemically modified chitosan beads from aqueous solution. *Carbohydrate Polymers*, *83*, 1082–1087.

Reddad, Z., Gerente, C., Andres, Y., & Le Cloirec, P. (2002). Adsorption of several metal ions onto a low-cost biosorbent: Kinetic and equilibrium studies. *Environmental Science & Technology*, *36*, 2067–2073.

Saito, H., Tabeta, R., & Ogawa, K. (1987). High-resolution solid-state carbon-13 NMR study of chitosan and its salts with acids: Conformational characterization of polymorphs and helical structures as viewed from the conformation-dependent carbon-13 chemical shifts. *Macromolecules*, *20*, 2424–2430.

So, H. H., Cho, J. W., & Sahoo, N. G. (2007). Effect of carbon nanotubes on mechanical and electrical properties of polyimide/carbon nanotubes nanocomposites. *European Polymer Journal*, *43*, 3750–3756.

Sousa, F. W., Oliveira, A. G., Ribeiro, J. P., Rosa, M. F., Keukeleire, D., & Nascimento, R. F. (2010). Green coconut shells applied as adsorbent for removal of toxic metal ions using fixed-bed column technology. *Journal of environmental management*, *91*(8), 1634–1640.

Thomas, H. C. (1944). Heterogeneous ion exchange in a flowing system. *Journal of the American Chemical Society*, *66*(10), 1664–1666.

Wan Ngah, W., Endud, C., & Mayanar, R. (2002). Removal of copper (II) ions from aqueous solution onto chitosan and cross-linked chitosan beads. *Reactive and Functional Polymers*, *50*, 181–190.

Yahaya, N., Latiff, M., Abustan, I., Bello, O., & Ahmad, M. (2011). Fixed-bed column study for Cu (II) removal from aqueous solutions using rice husk based activated carbon. *International Journal of Engineering & Technol*, *11*, 248–252.

Yoon, Y. H., & Nelson, J. H. (1984). Application of gas adsorption kinetics I. A theoretical model for respirator cartridge service life. *The American Industrial Hygiene Association Journal*, *45*(8), 509–516.

Zhou, L., Wang, Y., Liu, Z., & Huang, Q. (2009). Characteristics of equilibrium, kinetics studies for adsorption of Hg (II), Cu (II), and Ni (II) ions by thiourea-modified magnetic chitosan microspheres. *Journal of Hazardous Materials*, *161*, 995–1002.